Effects of Tissue-Specific Smoothing Approaches on Statistical Analysis in Quantitative MRI

Antoine Jacquemin[1] and Christophe Phillips[1]

[1]GIGA-CRC Human Imaging, University of Liège, Liège, Belgium

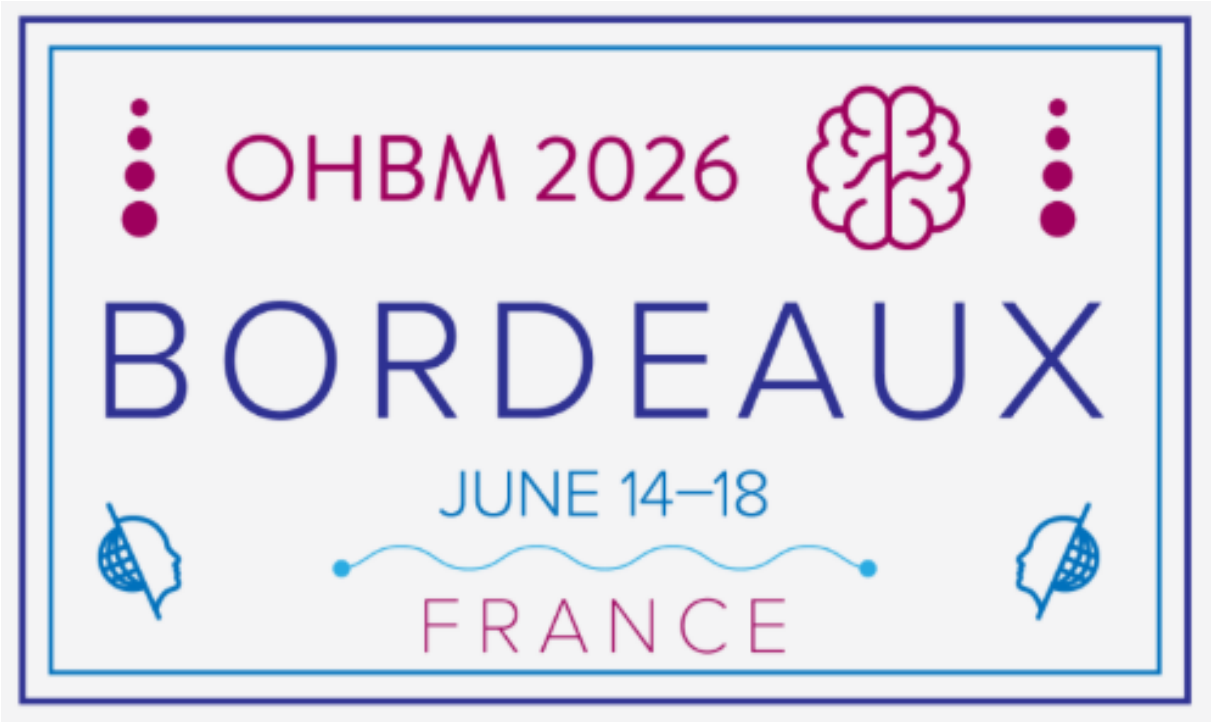

Introduction

Quantitative MRI (qMRI) provides voxel-wise maps of tissue properties sensitive to myelin, iron and water content, enabling in vivo assessment of microstructural changes. qMRI has, for example, been widely applied in aging studies, where it serves as a convenient framework for probing subtle tissue alterations across the lifespan. Previous voxel-wise and multivariate analyses have shown that aging is associated with coordinated alterations across multiple qMRI parameters[1], with multivariate models demonstrating higher sensitivity than univariate approaches in detecting subtle effects across gray matter (GM) and white matter (WM).[2]

However, when standard Gaussian kernel smoothing is applied, the interpretability of these maps can be compromised by partial volume effects, particularly at the boundaries between tissue classes such as GM and WM. To mitigate this issue, several **tissue-specific smoothing (TSmoo)** approaches have been proposed.

- In qMRI, Draganski et al. introduced a Linear, Gaussian, tissue-weighted and Compensated smoothing approach (TSmoo-LC).[3]

- For diffusion tensor imaging, Lee et al. proposed a WM-specific, Non-linear, Gaussian, tissue-masked and Compensated smoothing approach (TSmoo-NC).[4]
- For functional MRI, Smith et al. developed a Non-linear, tissue-masked, Intensity-weighted smoothing approach (TSmoo-NI) using the Smallest Univalue Segment Assimilating Nucleus (SUSAN).[5]

The objectives of this study are:

1. To extend the WM-specific TSmoo-NC approach to encompass both GM and WM, thereby broadening its applicability.
2. To systematically compare the impact of TSmoo-LC, TSmoo-NC and TSmoo-NI on quantitative MRI data, in order to evaluate their relative performance.

Methods

The TSmoo-NC approach, originally proposed by Lee et al.[4] was specific to white matter smoothing only. In the context of qMRI data, it was necessary to **generalize** the TSmoo-NC approach so that it could be applied to both GM and WM. To achieve this, tissue-specific masks (M_T) were generated for both GM and WM. Their generation is performed by applying the majority rule with a greater-than-20% probability criterion. The rationale is the following: the 20% threshold removes low-probability voxels, ensuring specificity by excluding noise and non-tissue contributions, then a voxel is included to M_T with the highest probability among GM, WM and cerebrospinal fluid (CSF), ensuring that each brain voxel is included in a single relevant M_T. These M_T are versatile and adaptable across different tissues and MRI modalities, making them broadly applicable in neuroimaging analyses.

With TSmoo-NC now generalized, the **mathematical formulations** of TSmoo-LC (*Eq.1*) , TSmoo-NC (*Eq.2*) and TSmoo-NI (*Eq.3a*) are presented in *Figure 1*, together with the corresponding equation legend. The parameter related to spatial smoothing was set to the same value across the three TSmoo approaches to allow comparison of their respective results. For TSmoo-NI, the parameter related to intensity was set to three-quarters of the median voxel intensities of each quantitative map. *Eq.3b* describes the functioning of SUSAN[5] but will be further discussed.

A qMRI **dataset** on normal aging was used to evaluate different smoothing approaches, which offers a convenient test case due to its well-characterized and subtle effects across brain tissue. The publicly available dataset comprises 138 healthy participants aged 19–75 years (mean age = 46.64, SD = 21), with 35.5% male `https://openneuro.org/datasets/ds005851/versions/1.0.0`. For each subject, the dataset provides quantitative maps of MTsat, PD, R1 and R2*, enabling voxel-wise assessment of multiple tissue properties relevant to microstructural characterization.

TSmoo-LC, TSmoo-NC and TSmoo-NI were used to **reproduce** the analysis from Callaghan et al.'s aging study[1], which relied on this dataset. The analysis, one per tissue class (GM and WM) and quantitative maps, consists in a GLM with 4 regressors (age, gender, total intracranial volume and scanner), where only the age effect is tested. These analyses enabled an objective and quantitative evaluation of the three smoothing approaches. The thresholded statistical parametric maps (SPMs; $p < 0.05$, FWE-corrected) derived from each method were systematically compared by quantifying the number of significant voxels and applying complementary statistical measures.

Additionally, voxelwise **log-likelihood (LL)** maps were computed to directly quantify the quality of the General Linear Model (GLM) fit under each smoothing method. LL provides a principled, model-based measure of goodness-of-fit that reflects how well the age-related effects are explained by the data at each voxel. For each smoothing approach, voxelwise LL was calculated from the residual variance and model predictions across subjects, ensuring full comparability across linear or non-linear TSmoo approaches. These LL maps were then used to assess whether differences in statistical sensitivity between smoothing strategies were associated with systematic differences in model fit quality, providing a complementary evaluation independent of thresholded SPMs.

Subsequently, **Bland–Altman** plots were applied to these LL maps to assess voxelwise agreement between smoothing strategies and to identify systematic biases in fit quality introduced by each TSmoo approach. Finally, the stationarity behavior of the three smoothing approaches was examined. Both the assumptions of stationarity and non-stationarity **random field theory** were explicitly tested and the resulting outcomes were compared to assess whether the inference remained consistent across different smoothness frameworks.

Figure 1: The mathematical formulations of TSmoo-LC (Eq.1), TSmoo-NC (Eq.2) and TSmoo-NI (Eq.3).

Eq. 1
$$TSMOO - LC(x) = \frac{(g * (\omega s(\phi)))(x)}{(g * \omega)(x)} \quad ; \quad \begin{cases} TPM > 0.05 \\ g * \omega > 0.05 \end{cases}$$

Eq. 2
$$TSMOO - NC(x) = \frac{(g * (M_T s(\phi)))(x)}{(g * M_T)(x)} \quad ; \quad g * M_T > 0.05$$

Eq. 3a
$$TSMOO - NI(x) = (susan * (M_T s(\phi)))(x)$$

Eq. 3b where:
$$susan(\mathbf{x}) = \frac{\sum_{\mathbf{p} \in N(\mathbf{x})} w(\mathbf{x}, \mathbf{p}) I(\mathbf{p})}{\sum_{\mathbf{p} \in N(\mathbf{x})} w(\mathbf{x}, \mathbf{p})}$$

$$\begin{cases} w(\mathbf{x}, \mathbf{p}) = c_b(\mathbf{x}, \mathbf{p}) \cdot c_s(\mathbf{x}, \mathbf{p}) \\ c_b(\mathbf{x}, \mathbf{p}) = \exp\left(- \left(\frac{I(\mathbf{p}) - I(\mathbf{x})}{bt} \right)^2 \right) \\ c_s(\mathbf{x}, \mathbf{p}) = \exp\left(- \frac{|\mathbf{p} - \mathbf{x}|^2}{2dt^2} \right) \end{cases}$$

Legend:

- $s(\phi)$ = quantitative map warped into standard space warped by ϕ
- ω = modulated tissue weigths warped in standard space constructed from $\omega = |\phi| t(\phi)$ where $|\phi|$ are the Jacobian determinants of deformation ϕ and $t(\phi)$ the tissue class image warped by ϕ
- M_T = "majority and greater than 20%" tissue-specific mask normalized in standard space warped by ϕ
- $g*$ = Gaussian isotropic smoothing convolution evaluated at x
- $susan*$ = SUSAN smoothing operator (Eq.3b).

Results

As expected the re-analysis of the same data but smoothed differently lead to different results. *Figure 2 (A/B/C)* shows statistical parametric maps identifying regions (red for GM and blue for WM) where R2* significantly increases with age at the $p < 0.05$ FWE-corrected level. The results are superimposed on the mean MTsat map for the cohort in MNI space. The four axial slices are located at z = -10, -2, 7 and 62 mm, from left to right.

TSmoo-LC and TSmoo-NC produce visually similar results (*Figure 2 A/B*). However, the number of significant voxels ($p < 0.05$ FWE) and the number of clusters they form are higher with TSmoo-LC than with TSmoo-NC for both GM and WM (*Figure 2 Table*). This can be explained by the effective smoothing averaged across the three FWHM dimensions, which is slightly higher with TSmoo-LC for both GM and WM compared to TSmoo-NC. This observation aligns with the fact that TSmoo-LC exhibits a lower number of resels than TSmoo-NC.

When examining the results from TSmoo-NI (*Figure 2 C*), they are markedly different from those of TSmoo-LC and TSmoo-NC (*Figure 2 A/B*), both visually and quantitatively. TSmoo-NI results in a much lower number of significant voxels and clusters compared to the other two TSmoo approaches (*Figure 2 Table*). Additionally, its average effective smoothing is approximately half that of TSmoo-LC and TSmoo-NC. Consistent with these observations, TSmoo-NI demonstrates a significantly higher number of resels than the other two TSmoo approaches.

Looking at the voxelwise log-likelihood (LL) maps (*Figure 2 D*), one can notice that TSmoo-NI leads to a better fit of the statistical model at the boundaries between GM and WM. Indeed, TSmoo-NI shows higher LL values at the sulci and gyri of the cortex. TSmoo-LC, on the other hand, shows a better GLM fit primarily within the gray matter, while TSmoo-NI proves to be superior in the core of the white matter.

Regarding the Bland-Altman plots, they reveal only minor mean biases across the different TSmoo methods, which are not included in this abstract. Moreover, the results obtained using the assumptions of stationarity or non-stationarity of random field theory are negligible for the TSmoo-LC and TSmoo-NC approaches. In contrast, the results of TSmoo-NI differ slightly. A reduction of about 2% in the number of resels is observed under the non-stationarity assumption.

These findings were consistent across all quantitative parameters: MTsat, PD, R1 and R2* (the first three are not shown).

Conclusion

Reproducing the age-related findings of Callaghan et al. (2014)[1] using three tissue-specific smoothing approaches revealed systematic and interpretable differences in statistical outcomes depending on the chosen TSmoo approach. TSmoo-LC and TSmoo-NC produced broadly comparable spatial patterns of age-related increases in R2*, consistent with the original study[1], yet TSmoo-LC yielded a notably higher number of significant voxels and clusters. This difference can be attributed to the slightly higher effective smoothing achieved with TSmoo-LC, which reduces the number of resels and consequently increases statistical sensitivity. The similarity between TSmoo-LC and TSmoo-NC suggests that both linear and nonlinear tissue modulation preserve the essential spatial features of the underlying signal when the effective smoothness is comparable.

In contrast, TSmoo-NI produced results that differed markedly from the other two ap-

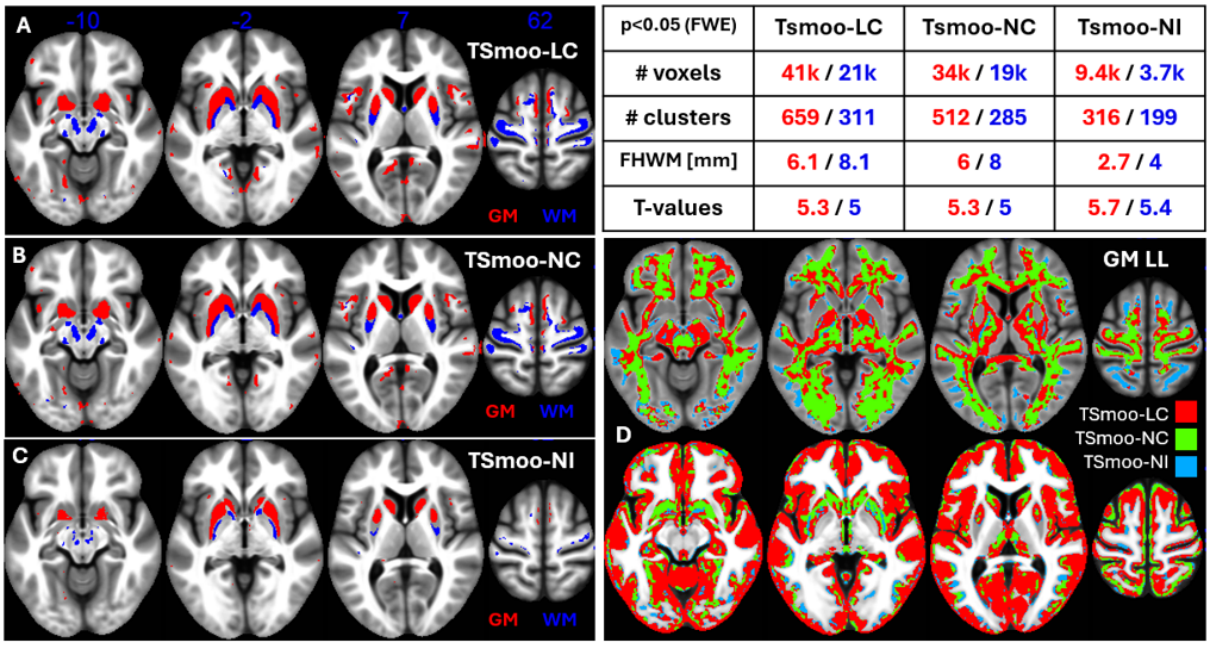

p<0.05 (FWE)	Tsmoo-LC	Tsmoo-NC	Tsmoo-NI
# voxels	41k / 21k	34k / 19k	9.4k / 3.7k
# clusters	659 / 311	512 / 285	316 / 199
FHWM [mm]	6.1 / 8.1	6 / 8	2.7 / 4
T-values	5.3 / 5	5.3 / 5	5.7 / 5.4

Figure 2: (A/B/C) Statistical parametric maps identifying regions (red for GM and blue for WM) in which R2* significantly increased (AR+) with age at the p < 0.05 FWE corrected level. The results are superimposed on the mean MT map for the cohort in MNI space. The four axial slices are located at z = −10, -2, 7 and 62 mm, from left to right. The table shows the corresponding statistical results (i.e., the number of statistically significant voxels and clusters, the averaged effective smoothing, and the statistical thresholds T-values). (D) The R2 log-likelihood maps for gray matter (top) and for white matter (bottom). The four axial slices are located at z = −10, -2, 7 and 62 mm, from left to right.

proaches. TSmoo-NI showed substantially fewer significant voxels and clusters, which reflects its considerably lower effective smoothness - approximately half that of TSmoo-LC and TSmoo-NC. This reduced smoothing led to a larger number of resels and, consequently, a more conservative statistical outcome. Unlike TSmoo-LC and TSmoo-NC, TSmoo-NI includes intensity modulation (*Eq.3a*). This modulation preserves local contrast and sharp transitions between gray and white matter, which helps to retain anatomical detail that conventional smoothing tends to blur.

The voxelwise log-likelihood maps further support this interpretation. TSmoo-NI provided a better GLM fit at the GM–WM boundaries, particularly within sulcal and gyral transitions. The intensity-modulated smoothing preserves these sharp gradients, enabling the model to capture subtle spatial variations more accurately. TSmoo-LC, in contrast, showed better model fit in cortical gray matter, while TSmoo-NC performed better in deep white matter. This suggests that the continuous tissue weighting in TSmoo-LC (*Eq. 1*) may better capture small variations within gray matter, whereas the binary tissue mask used in TSmoo-NC (*Eq. 2*) is more suited to the homogeneity of the white-matter core.

This study demonstrates that the choice of tissue-specific smoothing strategy critically influences both statistical sensitivity and model fit in voxelwise quantitative MRI analyses. These findings underline the importance of carefully selecting a TSmoo approach based on the scientific objective: maximizing detection power versus preserving anatomical specificity.

All scripts used in this study are available at: `https://github.com/CyclotronResearchCentre/TissueSpecificSmoothing`.

References

1. Callaghan MF, Freund P, Draganski B, et al. Widespread age-related differences in the human brain microstructure revealed by quantitative magnetic resonance imaging. Neurobiol Aging. 2014;35(8):1862-1872. doi:10.1016/j.neurobiolaging.2014.02.008

2. Moallemian S, Bastin C, Callaghan MF, Phillips C. Multivariate age-related analysis of variance in quantitative MRI maps: Widespread age-related differences revisited. medRxiv. Published online October 20, 2023.
doi:10.1101/2023.10.19.23297253

3. Tabelow K, Balteau E, Ashburner J, et al. hMRI—a toolbox for quantitative MRI in neuroscience and clinical research. Neuroimage. 2019;194:191-210. doi:10.1016/j.neuroimage.2019.01.029

4. Lee JE, Chung MK, Lazar M, et al. A study of diffusion tensor imaging by tissue-specific, smoothing-compensated voxel-based analysis. Neuroimage. 2009;44(3):870-883.
doi:10.1016/j.neuroimage.2008.09.041

5. Smith SM, Brady JM. SUSAN—A new approach to low-level image processing. Int J Comput Vis. 1997;23(1):45-78. doi:10.1023/a:1007963824710